μ-ANALYSIS APPLIED TO SELF-SENSING ACTIVE MAGNETIC BEARINGS

P.A. van Vuuren * **and G. van Schoor** †

* *School of Electrical, Electronic and Computer Engineering, North-West University, Private Bag X6001, Potchefstroom, 2520, South-Africa. E-mail: Pieter.VanVuuren@nwu.ac.za*

† *E-mail: George.vanSchoor@nwu.ac.za*

Abstract: The stability margin of a two degree-of-freedom self-sensing active magnetic bearing (AMB) is estimated by means of μ-analysis. The specific self-sensing algorithm implemented in this study is the direct current measurement method. Detailed black-box models are developed for the main subsystems in the AMB by means of discrete-time system identification. In order to obtain models for dynamic uncertainty in the various subsystems in the AMB, the identified models are combined to form a closed-loop model for the self-sensing AMB. The response of this closed-loop model is then compared to the original AMB's response and models for the dynamic uncertainty are empirically deduced. Finally, the system's stability margin for the modelled uncertainty is estimated by means of μ-analysis. The results show that μ-analysis is ill-equipped to estimate the stability margin of a nonlinear system.

Key words: Active magnetic bearings, system identification, self-sensing, μ-analysis

1. INTRODUCTION

In contrast with conventional bearings, active magnetic bearings (AMBs) use actively controlled magnetic forces to ensure contactless support of a rotating axle. An AMB consists of non-contact position sensors, a digital controller, power amplifiers and a stator with electromagnets. These components and the general structure of an AMB are summarized in [1].

Accurate and reliable position sensors form critical components of a functioning AMB system. These sensors are however expensive. Self-sensing techniques attempt to estimate the position of the rotor from the electrical impedance of the stator electromagnet coils [2].

For self-sensing AMBs to be of practical worth, they have to be robust. Robustness analysis aims to quantify a control system's tolerance for uncertainty. This uncertainty in general encompasses any deviation of the mathematical model from the physical reality. Uncertainties surrounding the model can be broadly classified into parametric uncertainty and dynamic uncertainty. Parametric uncertainty is applicable when the system's model is accurate with the exception of a few parameters whose precise values aren't known [3]. In contrast, dynamic uncertainty describes the situation when the system's model is inaccurate due to unmodelled dynamics [3].

The *de facto* standard for robustness estimation in the AMB literature is the sensitivity function [4], [5] and [6]. Acceptance of the draft ISO standard* for the evaluation of the stability of rotating machinery equipped with AMBs [7] isn't unanimous in the AMB research community. In [8] it is argued that the peak value of the sensitivity function only gives a necessary (but not sufficient) condition for robust stability. Their theoretical arguments were also supported by practical examples of AMB suspended systems that met the criteria set out by the draft ISO standard, yet became unstable due to modal variations or gyroscopic coupling.

Alternative multiple-input, multiple-output (MIMO) robustness estimation techniques that have been applied to AMBs include the generalized Nyquist criterion [9], Kharitonov's stability theorem [9] and the ν-gap metric [10]. Of the available LTI MIMO robustness estimation techniques, μ-analysis holds out the promise of delivering the least conservative estimates of the stability margin of an AMB system. Although μ-synthesis has been applied to design controllers for AMB systems (e.g. [11] and [10]), μ-analysis curiously has never been used to assess the robustness of AMBs.

Robustness analysis techniques have played a pivotal role in the debate on the viability of self-sensing AMBs. After the development of state-estimator self-sensing AMBs, Kucera showed by means of a sensitivity analysis that such self-sensing AMBs are quite sensitive for parametric uncertainty [12]. Following this result, Morse *et al.* used the sensitivity function to prove that self-sensing in general has fundamental theoretical limits on its stability robustness [13]. These negative results were however soon contradicted by various researchers (e.g. [4]) who showed that practical modulation based self-sensing AMBs can be almost as robust as sensed AMBs (according to the proposed ISO standard).

The apparent contradiction between the theory and practical results on the robustness of self-sensing AMBs was addressed by Maslen *et al.* [14] and [15]. They found that it is essential to include the switching ripple

*This draft standard uses the sensitivity function to assess the robustness of AMBs.

component of the coil current in the AMB model that is subjected to robustness analysis. Accurate modelling of switching power amplifiers requires nonlinear time-variant models.

One of the lessons from [13], [14] and [15] is that accurate robustness analysis requires that each of the constituent parts of a self-sensing AMB system be modelled accurately. The fundamental prerequisite for μ-analysis is however that the system under scrutiny be modelled with an *analytical LTI* model. Fortunately, it is possible for LTI black-box models obtained via system identification to closely approximate the oscillatory behaviour of switching power amplifiers if the order is chosen sufficiently high. Another advantage of system identification is that it doesn't have any trouble in modelling cross-coupling occurring in a system. This is a huge benefit since electromagnetic cross-coupling also has a large effect on self-sensing implemented on heteropolar AMBs [16], [5]. Furthermore, it is quite difficult to obtain an accurate analytical model for electromagnetic cross-coupling in an AMB stator by means of first principles deductive modelling techniques. The potential pitfalls of applying system identification to AMBs are highlighted in [1]. The most important lesson from [1] is that the excitation signal used for system identification must be constructed wisely in order to ensure that an *LTI* model is obtained.

Robustness analysis of self-sensing AMBs by means of μ-analysis therefore requires that detailed black-box models are developed for the main subsystems in the AMB by means of discrete-time system identification. Accurate μ-analysis requires accurate models of the nominal system as well as the uncertainty to which the model is subjected [3]. For this reason system identification is also applied to obtain accurate models for the dynamic uncertainty in the self-sensing AMB system.

Although the basic idea (namely of performing μ-analysis on the basis of models obtained via system identification) isn't new, it is the first time that it has been applied to self-sensing AMBs. The closest prior work in this general field was however confined to SISO systems in the process control industry [17], [18].

This paper's focus is on a 2-DOF *self-sensing* AMB. The dependency of self-sensing on an accurate representation of the ripple current in turn requires that the self-sensing module, AMB plant and power ampifier models be separately obtained by means of system identification. This is in contrast with the standard practice of system identification in the AMB literature, namely of including everything except the controller in the plant model [19], [20], [21] and [22].

The rest of this paper starts off with a summary of the specific version of self-sensing under scrutiny, namely the direct current measurement (DCM) method. Section 3 discusses the application of system identification to obtain discrete-time models for each of the main components

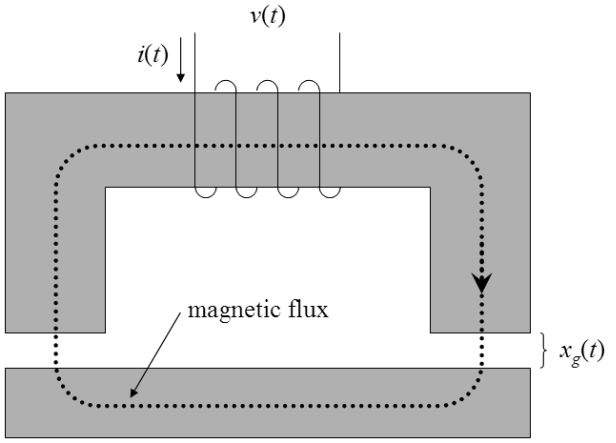

Figure 1: Magnetic circuit of a 1-DOF AMB

of the self-sensing AMB. Next, section 4 summarizes the application of μ-analysis by means of a case study, namely the robustness analysis of the AMB for dynamic uncertainty in the self-sensing module. Following this, the procedure with which dynamic uncertainty in the AMB plant and self-sensing module can be modelled is briefly described in section 5. Lastly, section 6 contains the results of simulation studies on μ-analysis applied to assess the effect of various forms of uncertainty on the stability margin of the self-sensing AMB.

2. THE DCM SELF-SENSING AMB

2.1 Introduction to DCM self-sensing

Self-sensing capitalizes on the principle that the inductance of an AMB stator coil is influenced by the size of the airgap. To see how the impedance of an AMB coil is influenced by the airgap take for example the magnetic circuit of a one degree-of-freedom (1-DOF) AMB in figure 1 [4].

To simplify the analysis, eddy current effects are neglected (as well as magnetic leakage and fringing). Furthermore, it is assumed that the magnetic flux has a uniform distribution throughout the magnetic circuit. By making use of the laws of Faraday, Ohm and Ampere, the relationship between the coil voltage $v(t)$ and current $i(t)$ is given by (1) [23],

$$v(t) = \left(\frac{\mu_0 N^2 A}{2x_g(t)+l_c/\mu_r}\right)\frac{di(t)}{dt} - 2\left(\frac{\mu_0 N^2 A i(t)}{(2x_g(t)+l_c/\mu_r)^2}\right)\frac{dx_g(t)}{dt} + i(t)R, \quad (1)$$

where μ_0 is the permeability of free space; N is the number of turns in the coil; A is the pole-face area; x_g is the distance of the airgap between the stator and rotor; l_c is the length of the magnetic path (excluding the airgap); μ_r is the relative permeability of the AMB stator; and R denotes the electrical resistance of the coil wire.

Clearly, the relationship between the coil voltage and current is influenced by the instantaneous position of the rotor within the airgap.

DCM self-sensing stems from the fact that the rotor position is directly related to the peak value of the ripple current during a switching cycle. This becomes obvious when (1) is simplified further to its bare essentials. By neglecting the coil resistance, as well as nonlinear magnetic effects and assuming that the AMB rotor moves very slowly compared to the rapid variation in the coil current, the airgap can be expressed as follows [5]:

$$x_g(t) = \left(\frac{\mu_0 N^2 A}{2v(t)}\right)\frac{di(t)}{dt} - \frac{l_c}{\mu_r}. \qquad (2)$$

From (2) it is clear that the airgap can be estimated from a direct measurement of the peak ripple current value. More details on how DCM self-sensing compensates for magnetic nonlinearities and the duty cycle of the power amplifiers can be found in [5] and [24].

2.2 *Simulation platform*

This paper's results are based on simulation studies performed with a reasonably accurate simulation model of a two degree-of-freedom (2-DOF) DCM self-sensing AMB. (The accuracy of this simulation model and its components has been established in [6] and [5].) The small inaccuracies of the self-sensing AMB simulation model (as compared to the eventual physical implementation) can be attributed to unmodelled behaviour in the electronic circuitry of the hardware implementation. The above mentioned simulation model consists of a controller, four power amplifiers, a magnetic circuit model, point mass and ideal position sensors. Two identical PID controllers (each responsible for movement along one axis of freedom) comprise the controller, while each of the four stator electromagnets is powered by its own two-state switching power amplifier.

The flux distribution in the AMB magnetic circuit is modelled by means of a reluctance network model [25]. The response of the reluctance network model is enriched with two additional models: one responsible for predicting eddy currents and the other for modelling magnetic hysteresis and saturation. The final electromagnetic force exerted by the AMB on the point mass is proportional to the square of the magnetic flux density [26], [6]. Finally, the physical movement of the point mass is determined by means of the well-known Newton laws.

The characteristic parameters of the simulated AMB are summarized in table 1 (some of which are explained in figure 2).

Table 1: Summary of the simulated self-sensing AMB

Parameter	Value
K_P (position PID controller)	20,000
K_I (position PID controller)	700,000
K_D (position PID controller)	38
K_P (power amplifier PI controller)	0.7
K_I (power amplifier PI controller)	0.01
Relative magnetic permeability	4,000
Power amplifier switching frequency	30 kHz
Supply voltage	50 V
Bias current	3 A
Resistance of coil wires	0.2 Ω
Coil turns	50
Rotor mass	3.86 kg
Airgap	0.6 mm
Backup bearing inner radius	250 μm
Axial bearing length	49.15 mm
Journal inner radius (r_r)	15.88 mm
Journal outer radius (r_j)	34.95 mm
Stator pole radius (r_p)	35.60 mm
Stator back-iron inner radius (r_c)	60.00 mm
Stator outer radius (r_s)	75.00 mm
Pole width (r_w)	13.89 mm

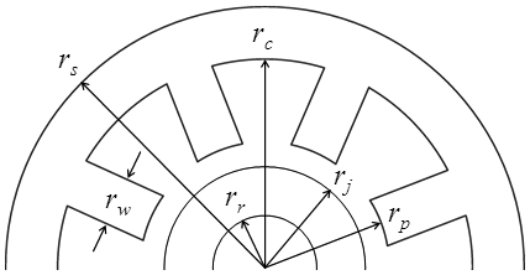

Figure 2: Physical dimensions of an AMB

3. SYSTEM IDENTIFICATION OF THE NOMINAL MODEL

Applying system identification to AMBs is a challenging exercise due to the inherent instability of magnetic bearings. Since open-loop operation of an AMB is impossible, system identification must be performed while the AMB is in closed-loop operation. More details on closed-loop system identification can be found in [27] and [1]. Other relevant system identification topics also discussed in [1] include: the influence of the injection point of the excitation signal; general parameterized model structures suitable for AMBs and their associated parameter estimation algorithms as well as the important topic of persistent excitation.

The main disadvantage of black-box modelling is that it gives limited insight into the internal dynamics of the real system. In the context of robustness analysis, this implies that it is difficult to apportion blame to specific system components when the total closed-loop system is fragile (and only a single model for the whole system is available). The solution to this problem is more detailed modelling where individual components in the control system are also modelled via system identification.

The main components in a 2-DOF self-sensing AMB

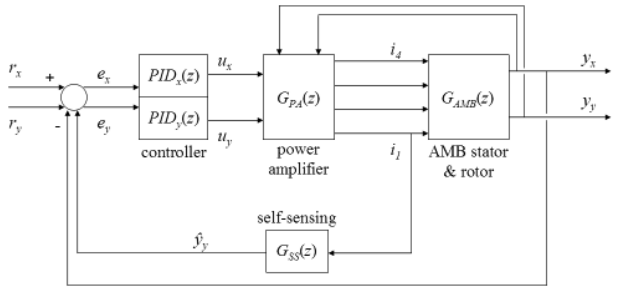

Figure 3: Block-diagram of an LTI self-sensing AMB

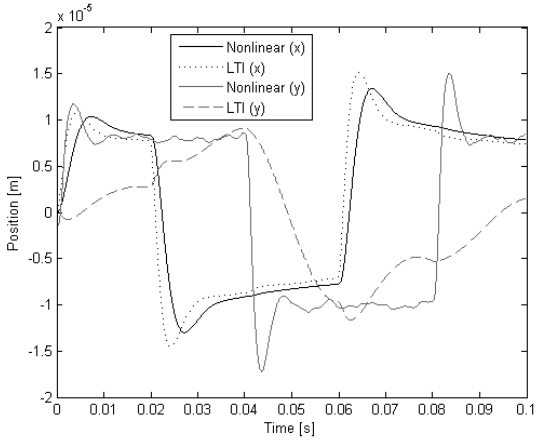

Figure 4: Performance of the nominal LTI closed-loop model

are the controller, power amplifiers, AMB plant and self-sensing module. A simplified block-diagram of a 2-DOF self-sensing AMB is given in figure 3. In this study the controller consists of two identical decoupled PID controllers, each responsible for the control of one axis of freedom.

The fundamental principle upon which self-sensing is based is that the impedance of the coils (specifically their inductance) is a function of the airgap [6]. This means that a power amplifier's response is not only a function of the controller output, but also of the actual position of the mass within the airgap. To ensure that the outputs of the LTI power amplifier model contain position information, the LTI model should be an explicit function of all variables that have an effect on the real coil currents (namely two outputs from the controller and two position signals from the output of the AMB plant).

The AMB model has four inputs (one for each electromagnet) and two outputs (namely the measured x-axis and y-axis position of the rotor). In order to evaluate the performance of the self-sensing algorithm, the x-axis rotor position is measured with an eddy-current position sensor, while DCM self-sensing is only implemented on the y-axis. DCM self-sensing (as implemented in [5]) only takes a single input (namely the current flowing in the top pair of coils) to form an estimate of the y-axis rotor position.

In contrast with the standard practice in the system identification literature, detrending is inadvisable when system identification is applied to self-sensing AMBs. This is because DCM self-sensing is sensitive for the bias current level in order to compensate for nonlinearity due to hysteresis and saturation in the magnetic material of the AMB stator [5]. Detrending would therefore result in loss of information on the necessary setpoint of the LTI self-sensing model, with subsequent delevitation of the rotor.

System identification works best if the sampling frequency is commensurate with the time constants of the plant [28]. DCM self-sensing however requires accurate measurements of the peak values of the modulated component present at the switching frequency of the power amplifiers (which is 30 kHz). This means that the eventual identified models must have sampling frequencies higher than 60 kHz at least. DCM self-sensing requires accurate measurements of the peak values of the switching ripple on the current signal. The risk of consistently missing the peak value of the current ripple is furthermore dramatically increased if the sampling frequency is close to being an integer multiple of the switching frequency. The final sampling frequency that met all of these requirements was 83.3 kHz.

The *de facto* procedure in μ-analysis is to convert the discrete-time model to an equivalent continuous-time model prior to calculating the values of μ. Since the latter conversion tends to amplify any errors made during discrete-time parameter estimation by a factor approximately equal to the sampling frequency [27], it is vitally important to obtain very accurate discrete-time models for the various AMB sub-components.

As an example, parameter estimation was performed on rectangular pulses injected prior to the power amplifiers in the nonlinear simulation model. The final nominal closed-loop LTI model of the 2-DOF self-sensing AMB of this study consisted of the following discrete-time state-space models ([27]): a 9^{th} order AMB plant model (4 inputs, 2 outputs); a 7^{th} order power amplifier model (4 inputs, 4 outputs) and a 3^{rd} order SISO model for DCM self-sensing. Figure 4 shows the responses of both the original nonlinear simulation as well as the closed-loop LTI model to a similar signal (but with a different amplitude). The x-axis performance of the LTI model is quite impressive (93.76 %), while the y-axis performance of 50.76 % is much less so. Clearly the identified self-sensing model is at fault, drastically reducing the bandwidth and fidelity of the total closed-loop system model. Poor performance of LTI models for nonlinear systems containing "hard" nonlinearities such as the maximum-operator used in DCM self-sensing is however to be expected.

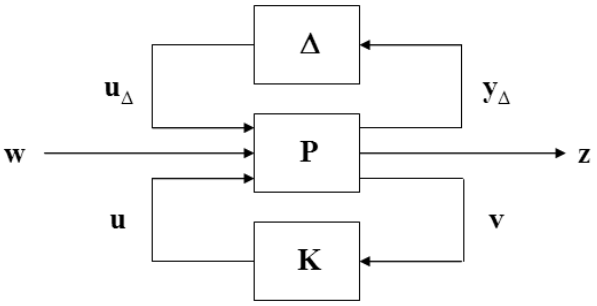

Figure 5: Generalized block diagram

4. APPLICATION OF μ-ANALYSIS TO THE DCM SELF-SENSING AMB

Robust control theory is built on the notion of norm-bounded uncertainty [29]. This is a frequency domain concept where the uncertainty surrounding a particular model can be expressed by means of bounds on the norm of the model's transfer function. The traditional system block-diagram can be rearranged to obtain the generalized form of figure 5 [3].

In this block-diagram the controller is represented by K, while the nominal model of the rest of the AMB system is collected in P (also known as the generalized plant). Δ is a block-diagonal matrix that consists of norm-bounded general uncertainties (scalars or LTI transfer functions conforming to respectively $|\Delta_m| \leq 1$ and $\|\Delta_n(j\omega)\|_\infty \leq 1 \ \forall \ \omega$, where the subscripts m and n refer to the corresponding elements in the block-diagonal matrix). The uncertainty matrix, Δ, therefore represents general uncertainties that can impact on the parameters or dynamics of the nominal generalized plant. The degree to which the general uncertainties in Δ actually influence the self-sensing AMB are determined by weights (whether scalar weights or weight transfer functions). These weights are incorporated into the generalized plant P.

For the purpose of μ-analysis, the controller K can be combined with the generalized plant P by means of a lower linear fractional transformation ([3]) to obtain (3).

$$\begin{bmatrix} y_\Delta \\ z \end{bmatrix} = N \begin{bmatrix} u_\Delta \\ w \end{bmatrix} = \begin{bmatrix} N_{11} & N_{12} \\ N_{21} & N_{22} \end{bmatrix} \begin{bmatrix} u_\Delta \\ w \end{bmatrix} \quad (3)$$

The last step of μ-analysis is then to isolate the N_{11} component and to determine its structured singular value (μ). If the peak value of $\mu_\Delta(j\omega)$ is less than one for all frequencies, then the difference between one and the aforementioned peak value reflects the stability margin of the system.

An example of dynamic uncertainty in self-sensing AMBs is the unmodelled dynamics that occur if DCM self-sensing is modelled by means of LTI system identification. We'll assume that the dynamic uncertainty in DCM self-sensing can be modelled with additive

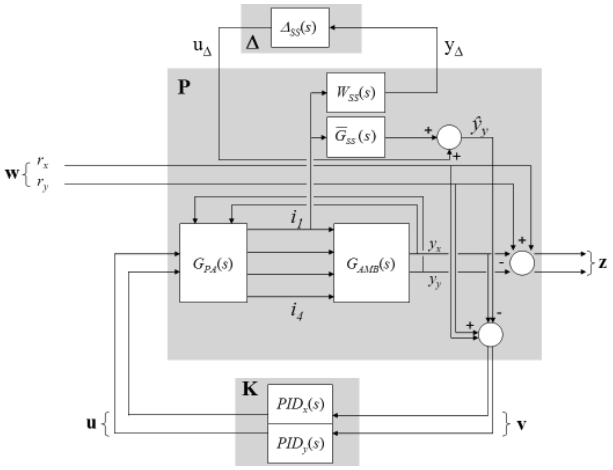

Figure 6: Detailed generalized block-diagram of a self-sensing AMB with dynamic uncertainty in the self-sensing module

uncertainty. An improved LTI model that attempts to model the behaviour of DCM self-sensing more accurately, is the following additive combination between the nominal LTI self-sensing model $\bar{G}_{SS}(s)$ and the LTI uncertainty weight function for self-sensing, $W_{SS}(s)$:

$$G_{SS}(s) = \bar{G}_{SS}(s) + W_{SS}(s)\Delta(s). \quad (4)$$

The resulting generalized block-diagram of a self-sensing AMB with additive dynamic uncertainty in the self-sensing module is given by figure 6. All that remains to be done is to obtain a model for the additive dynamic uncertainty present in the self-sensing module (i.e. to obtain a specific model for the transfer function $W_{SS}(s)$), which is the topic of the next section.

5. UNCERTAINTY MODELLING

The dominant contributor towards dynamic uncertainty in self-sensing AMBs is the occurrence of nonlinear behaviour that can't be modelled in the LTI paradigm. The process of modelling this mismatch entails a two step process [30], [31]. Firstly, the "difference" between the model and real system is measured empirically. Secondly, the measured differences are described by means of a simplified transfer function.

The "difference" between the model and real system can be expressed in terms of an empirical transfer function estimate (ETFE) of the measured mismatch between the real plant and its nominal model. The advantage of a frequency domain comparison between reality and the model is that it isn't necessary to use exactly the same input signal for the real system and its nominal model (in contrast with time domain residuals).

The general norm-bounded uncertainty $\Delta(s)$ in (4) is constrained as follows: $\|\Delta(j\omega)\|_\infty \leq 1 \ \forall \ \omega$, where the H_∞-norm is defined as follows for any proper and stable

transfer function $G(s)$ [3]:

$$\|G(j\omega)\|_\infty = \sup_\omega |G(j\omega)| \tag{5}$$

Consequently, the ETFE of the uncertainty weight for additive uncertainty must conform to the following inequality:

$$|W(s)| \geq \left| \frac{Y(s)}{X(s)} - \frac{\bar{Y}(s)}{\bar{X}(s)} \right|, \tag{6}$$

where the spectra of the input and output signals of the real system are represented by $X(s)$ and $Y(s)$ respectively. Similarly, the input and output spectra of the nominal model are given by $\bar{X}(s)$ and $\bar{Y}(s)$ respectively.

To summarize, the procedure for obtaining the ETFE of the uncertainty weight is as follows:

1. Form a closed-loop LTI model for the AMB system consisting of nominal LTI state-space models for the controller, power amplifier, AMB plant and self-sensing module.
2. Apply the same position reference signal to both the nonlinear AMB simulation model and the closed-loop LTI model and simulate the responses of both models.
3. Calculate the ETFE of the SISO uncertainty weight by means of (6). This will result in the measured uncertainty weight for dynamic uncertainty in the self-sensing module. By a similar calculation the ETFEs of the uncertainty weights for additive dynamic uncertainty in the other subsystems (namely the power amplifier and the AMB plant) can also be obtained.

The second step of the uncertainty modelling process entails summarizing the above mentioned ETFE by means of an analytical model. The *de facto* practice in the literature is to fit a smooth function which acts as an upper bound to the measured frequency response [3], [31] and [30]. Various means exist to accomplish this purpose. One potential solution entails finding a number of peaks in the ETFE and connect them with low order curves. The result is a piecewise continuous curve that closely approximates the original ETFE, yet is much smoother. Finally, zeros and poles are iteratively added in accordance with the well-known first order asymptotic approximations for Bode plots until the deviation between the observed ETFE and the fitted function is below a predefined threshold. More details on this algorithm can be found in [27].

As an example, the effect of dynamic uncertainty occuring in the self-sensing module on the closed-loop system's stability margin can be assessed as follows. First of all, a random-phase multi-sine signal (with an amplitude of 100 μm and frequency content stretching from 5 Hz to 26 Hz) is applied to the system input. The choice of this excitation signal is motivated by the existence

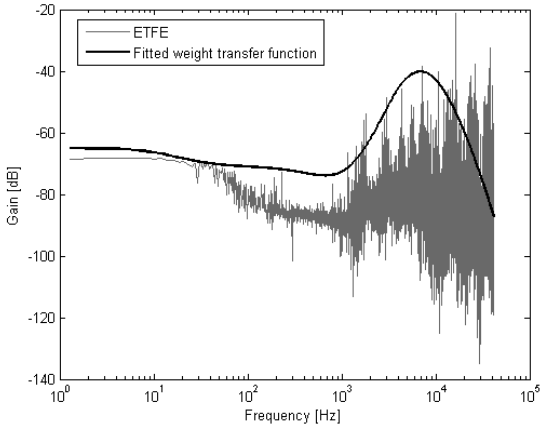

Figure 7: Uncertainty weight ETFE and bounding function for dynamic additive uncertainty in the self-sensing module

of frequency-induced nonlinear behaviour in AMBs [1]. From this excitation signal the additive uncertainty weight in figure 7 is estimated. A maximum of 3 dB deviation was allowed between the piecewise continuous upper bound (not shown) and the fitted transfer function, with the added constraint that the fitted function must be a strictly proper transfer function. According to the modelled uncertainty, the nominal LTI self-sensing model's primary shortcoming is its high-frequency behaviour. Nonetheless, the generally low gain levels of the uncertainty weight are indicative of a relatively accurate LTI model for the self-sensing module.

6. RESULTS

6.1 Validation procedure

An important topic that rarely attracts any attention in the robust control literature is the validation of the uncertainty models used as well as the final stability margins estimated by μ-analysis. Validation of a model for dynamic uncertainty basically entails assessing whether the uncertainty model is truly an accurate representation of the unmodelled effects in the original system as modelled by the nominal model.

The tack that will be taken in this paper is loosely based on some of the ideas in [32] and [33]. Essentially, an uncertainty model would be valid if it could be used along with the original nominal model to duplicate the behaviour of the nonlinear system. In other words, a new LTI closed-loop system model is synthesized from the nominal models identified during system identification, as well as the fitted uncertainty weighting functions. (The norm-bounded uncertainty, $\Delta(s)$, which usually accompanies the uncertainty weight, is now taken as the all-pass function.) The response of the resultant LTI model can then be calculated for any particular input signal. By comparing the response of the new closed-loop LTI model (known as the *augmented* model) with the corresponding response of the nonlinear system, it is

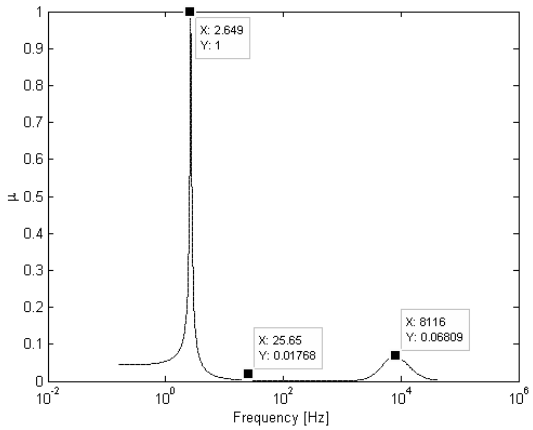

Figure 8: μ-plot for dynamic uncertainty in the self-sensing module

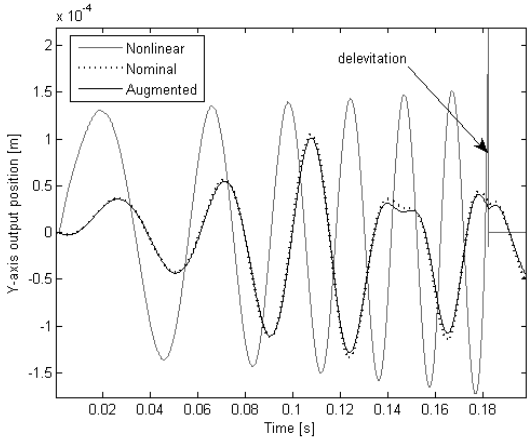

Figure 9: Responses to a frequency sweep

possible to qualitatively and quantitatively measure the accuracy of the uncertainty model.

The stability margin estimated by μ-analysis can be valdated by applying a sine-sweep test signal to both the augmented model and the original nonlinear simulation model. The specific frequency at which delevitation occurs (due to frequency-induced nonlinear behaviour in the AMB) is also a convenient measure of the stability margin of both the augmented model and the nonlinear simulation. The stability margin predicted by μ-analysis will be indirectly validated if both the augmented model and the nonlinear simulation model delevitate at similar frequencies of the input frequency sweep signal.

6.2 Robustness analysis for dynamic uncertainty in DCM self-sensing

Previous sections have detailed the nominal LTI model for a DCM self-sensing AMB as well as a model for unmodelled dynamics in the self-sensing algorithm. The unmodelled dynamics are specifically due to frequency-induced nonlinear behaviour in the AMB. All that remains is to calculate the value of μ and estimate the system's stability margin (by means of the Robust Control Toolbox in Matlab®).

In order to obtain useful results, the uncertainty weight function in figure 7 had to be be scaled down by a factor of 0.0012. Such a large scaling factor is indicative of the conservatism of μ-analysis for this specific application. The resultant μ-plot is shown in figure 8. Even though a 2 Hz component isn't visible in the uncertainty weight in figure 7, this component is the dominant factor in the μ-plot. From the μ-plot we can deduce that the closed-loop system's stability margin for dynamic uncertainty in the self-sensing module is dominated by an extreme sensitivity for the critical frequency of the AMB plant. The robustness of a self-sensing AMB for general dynamic uncertainty can therefore be improved by better control at this frequency.

The LTI uncertainty model is however totally unsuited to analyse the effect of nonlinear phenomena on the stability margin of the self-sensing AMB. This is proved by applying a 99 μm amplitude frequency sweep signal stretching from 11 Hz to 50 Hz at the system input. Such an input signal is guaranteed to induce nonlinear behaviour in the AMB as well as eventual delevitation [1]. As figure 9 clearly shows, neither the nominal LTI closed-loop model, nor the augmented model could correctly predict the frequency-induced delevitation occurring just after 0.18 seconds.

7. CONCLUSION

The fundamental issue uncovered in this paper is the validity of modelling a mismatch between a *nonlinear* system and an *LTI* nominal model by means of *another LTI* model (the uncertainty model). An example of this problem is the inability of μ-analysis to predict delevitation due to frequency induced nonlinearities in the AMB (e.g. in figure 9). Since the augmented model couldn't correctly model frequency-induced nonlinear behaviour in the AMB, the prime cause of the problem lies at the door of the LTI uncertainty weight.

Nonetheless, the μ-plot obtained for dynamic uncertainty in the self-sensing AMB is quite useful to identify specific frequencies where the system is especially fragile (and where the controller's performance has to be optimised).

Self-sensing AMBs are nonlinear multivariable systems. This paper has shown that a linearization approach to the robustness analysis of this system results in inaccurate robustness estimates. Accurate robustness analysis requires accurate models of the nominal system and the expected uncertainty. A good model for robustness analysis purposes must mimic all aspects of the true system's behaviour. Not only should the model replicate the system in well-behaved cases, but also when the system is teetering on the edge of instability. Further work should therefore be done on the development of an analytical nonlinear model for a self-sensing AMB and obtaining robustness estimates for the system by means of nonlinear

analysis techniques.

REFERENCES

[1] P. Van Vuuren, G. Van Schoor, and W. Venter, "LTI modelling of active magnetic bearings by means of system identification," *SAIEE Africa Research Journal*, vol. 102, no. 3, September 2011.

[2] E. Maslen, "Magnetic bearing sensors," in *Short course on magnetic bearings*, 1997.

[3] S. Skogestad and I. Postlethwaite, *Multivariable feedback control: analysis and design*, 2nd ed. Chichester, UK: John Wiley & Sons, 2005.

[4] A. Schammass, "A self-sensing active magnetic bearing: modulation approach," Ph.D. dissertation, EPFL, Switzerland, 2003.

[5] A. Niemann, "Self-sensing algorithms for active magnetic bearings," Ph.D. dissertation, North-West University, 2008.

[6] E. Ranft, "An improved model for self-sensing heteropolar active magnetic bearings," Ph.D. dissertation, North-West University (Potchefstroom campus), 2007.

[7] "1st ISO/CD 14839-3 "Mechanical vibration vibration of rotating machinery equipped with active magenetic bearings part 3: Evaluation of stability margin"," International Organization for Standardization, Committee draft standard ISO/TC 108 / SC 2, October 2003.

[8] G. Li, E. H. Maslen, and P. Allaire, "A note on ISO AMB stability margin," in *Proceedings of the 10th International Symposium on Magnetic Bearings*, Martigny, Switzerland, 2006.

[9] N.-C. Tsai, C.-H. Kuo, and R.-M. Lee, "Regulation on radial position deviation for vertical amb systems," *Mechanical Systems and Signal Processing*, vol. 21, pp. 2777–2793, 2007.

[10] G. Li, "Robust stabilization of rotor-active magnetic bearing systems," Ph.D. dissertation, University of Virginia, 2007.

[11] A. Lanzon and P. Tsiotras, "A combined application of H_∞ loop shaping and μ-synthesis to control high-speed flywheels," *IEEE Transactions on control systems technology*, vol. 13, no. 5, pp. 766–777, September 2005.

[12] L. Kucera, "Robustness of self-sensing magnetic bearing," in *Proceedings of MAG'97: Industrial conference and exhibition on magnetic bearings*. Alexandria, VA: Technomic, 1997, pp. 261–270.

[13] N. Morse, R. Smith, B. Paden, and J. Antaki, "Position sensed and self-sensing magnetic bearing configurations and associated robustness limitations," in *Proceedings of the 37th IEEE conference on decision and control*, December 1998, pp. 2599–2604.

[14] E. Maslen, D. Montie, and T. Iwasaki, "Robustness limitations in self-sensing magnetic bearings," *Journal of dynamic systems, measurement, and control*, vol. 128, pp. 197–203, June 2006.

[15] E. Maslen, T. Iwasaki, and R. Mahmoodian, "Formal parameter estimation for self-sensing," in *Proceedings of the tenth international symposium on magnetic bearings*, Martigny, Switzerland, August 21-23 2006.

[16] N. Skricka and R. Markert, "Influence of cross-axis sensitivity and coordinate coupling on self-sensing," in *Proceedings of 6th International Symposium on Magnetic Suspension Technology*, Turin, Italy, October 2001, pp. 179–184.

[17] K. Jun, D. Rivera, E. Elisante, and V. Sater, "A computer-aided design tool for robustness analysis and control-relevant identification of horizon predictive control with application to a binary distillation column," *Journal of Process Control*, vol. 6, no. 2/3, pp. 177–186, 1996.

[18] M. Kamrunnahar, D. Fisher, and B. Huang, "Performance assessment and robustness analysis using an armarkov approach," *Journal of Process Control*, vol. 14, pp. 915–925, 2004.

[19] C. Gähler, M. Mohler, and R. Herzog, "Multivariable identification of active magnetic bearing systems," *JSME international journal. Series C, Mechanical systems, machine elements and manufacturing*, vol. 40, no. 4, pp. 584–592, 1997.

[20] N. Gibson, H. Choi, and G. Buckner, "H_∞ control of active magnetic bearings using artificial neural network identification of uncertainty," in *2003 IEEE International Conference on Systems, Man and Cybernetics*, vol. 2, Washington D.C., 2003, pp. 1449–1456.

[21] H. Choi, G. Buckner, and N. Gibson, "Neural robust control of a high-speed flexible rotor supported on active magnetic bearings," in *Proceedings of the 2006 American Control Conference*, Minneapolis, Minnesota, June 2006, pp. 3679–3684.

[22] J. Sawicki, E. Maslen, and K. Bischof, "Amb controller design for a machining spindle using μ-synthesis," in *Proceedings of the tenth international symposium on magnetic bearings*, Martigny, Switzerland, August 21-23 2006.

[23] E. Maslen, "Self-sensing for active magnetic bearings: overview and status," in *Proceedings of the tenth international symposium on magnetic bearings*, Martigny, Switzerland, August 21-23 2006.

[24] A. Niemann and G. Van Schoor, "Self-sensing algorithm for active magnetic bearings; using direct current measurements," in *Proceedings of the 12th International Symposium on Magnetic Bearings*. Wuhan, China: ISMB, August 2010.

[25] D. Meeker, E. Maslen, and M. Noh, "An augmented circuit model for magnetic bearings including eddy currents, fringing, and leakage," *IEEE Transactions on Magnetics*, vol. 32, no. 4, pp. 3219–3227, July 1996.

[26] G. Schweitzer, H. Bleuler, and A. Traxler, *Active Magnetic Bearings: Basics, Properties and Applications of Active Magnetic Bearings*. Zürich: Authors Reprint, 2003.

[27] P. Van Vuuren, "Robustness estimation of self-sensing active magnetic bearings via system identification," Ph.D. dissertation, North-West University, 2010.

[28] L. Ljung, *System identification: theory for the user*, 2nd ed. Upper Saddle River, NJ: Prentice Hall, 1999.

[29] K. Zhou, J. Doyle, and K. Glover, *Robust and optimal control*. Upper Saddle River, NJ: Prentice Hall, 1996.

[30] D. Bayard, Y. Yam, and E. Mettler, "A criterion for joint optimization of identification and robust control," *IEEE Transactions on Automatic Control*, vol. 37, no. 7, pp. 986–991, July 1992.

[31] B. Lu, H. Choi, G. Buckner, and K. Tammi, "Linear parameter-varying techniques for control of a magnetic bearing system," *Control Engineering Practice*, vol. 16, pp. 1161–1172, 2008.

[32] R. Smith, "Model validation for robust control: an experimental process control application," *Automatica*, vol. 31, no. 11, pp. 1637–1647, 1995.

[33] H. Buckner, G.D. Choi and N. Gibson, "Estimating model uncertainty using confidence interval networks: applications to robust control," *Transactions of the ASME: Journal of dynamic systems, measurement, and control*, vol. 128, pp. 626–635, September 2006.